Transcriptional Characterization of the Stromal and Endothelial Bone Marrow Microenvironment during Progression from MGUS to Multiple Myeloma

Itziar Cenzano[1,2,*], Miguel Cócera[1,3,*], Azari Bantan[2], Marta Larrayoz[1], Amaia Vilas-Zornoza[1,3], Patxi San-Martin[1], Paula Aguirre-Ruiz[1], Diego Alignani[1,3], Aitziber Lopez[1], Marta Miñana Barrios[4], Delia Quilez Agreda[4], Ignacio Sancho González[5], Javier Ruiz[5], Vincenzo Lagani[2], Jesper Tegner[2,10,11,12], Ignacio Martín-Subero[6,7], Xabier Agirre[1,3], Bruno Paiva[1,3], Paula Rodriguez-Otero[3,8], Luis-Esteban Tamariz-Amador[3,8],Jesús San-Miguel[3,8], Jose A. Martinez-Climent[1,3], Borja Saez[1], Mikel Hernáez[3,9], Isabel A. Calvo[1,3,§], David Gomez-Cabrero[2,13,§], Felipe Prosper[1,3,8,§]

[1]Hematology and Oncology Program, Centre for Applied Medical Research (CIMA), Instituto de Investigaciones Sanitarias de Navarra (IdiSNA), Cancer Center Clinica Universidad de Navarra (CCUN), Pamplona, Navarra, Spain.
[2]Bioscience Program, Biological and Environmental Sciences and Engineering Division (BESE), King Abdullah University of Science and Technology KAUST, Thuwal 23955, Saudi Arabia.
[3]Centro de Investigacion Biomedica en Red de Cancer (CIBERONC). Madrid, Spain.
[4]Hospital Reina Sofía de Tudela, Navarra, Spain.
[5]Hospital Universitario de Navarra, Pamplona, Spain.
[6]Institut d'Investigacions Biomèdiques August Pi i Sunyer (IDIBAPS), Barcelona, Spain.
[7]Institució Catalana de Recerca i Estudis Avançats (ICREA), Barcelona, Spain.
[8]Hematology and Cell Therapy Department. Cancer Center Clinica Universidad de Navarra (CCUN), IdiSNA. Pamplona, Spain.
[9]Computational Biology Program. Cima Universidad de Navarra, Data Science and Artificial Intelligence Institute (DATAI) Universidad de Navarra, IdiSNA. Pamplona, Spain.
[10]Computer Science Program, Electrical and Mathematical Sciences and Engineering Division, King Abdullah University of Science and Technology (KAUST), Thuwal, 23955-6900, Kingdom of Saudi Arabia.
[11]Unit of Computational Medicine, Department of Medicine, Center for Molecular Medicine, Karolinska Institutet, Karolinska University Hospital, Stockholm, Sweden.
[12]Science for Life Laboratory, Solna, Sweden
[13]Translational Bioinformatics Unit, Navarrabiomed, Universidad Pública de Navarra (UPNA).

*These authors contributed equally to this work
[§]These authors jointly supervised this work

KEYWORDS
Multiple myeloma, single cell RNA sequencing, Endothelial cells, Stromal cells, tumor microenvironment.

CORRESPONDING AUTHOR
Felipe Prósper (fprosper@unav.es), David Gomez-Cabrero (david.gomezcabrero@kaust.edu.sa) and Isabel A. Calvo (icalvoa@unav.es).

ABSTRACT

Despite therapeutic advancements, Multiple Myeloma (MM) remains an incurable disease. To characterize the role that deregulation of the Bone Marrow (BM) microenvironment may have in the transition from healthy to Monoclonal Gammopathy of Undetermined Significance (MGUS), and from MGUS to MM, we performed single-cell RNA sequencing (scRNA-seq) of mesenchymal stromal cells (MSC) and endothelial cells (EC) from two mouse models, $BI_{c\gamma}$ and $MI_{c\gamma}$, that recapitulate the principal clinical, genetic, and immunological characteristics of MGUS and MM patients. Our results identify distinct transcriptional dynamics between MSC and EC. While EC acquires a stress state during MGUS, a proliferating and angiogenic profile characterizes MM. On the other hand, MSC compromised their differentiation potential, exhibiting a more inflammatory profile that initiates from the MGUS stage. Interestingly, we identified interferon (IFN)-related myeloma signature in malignant EC of the BIcγ model, which is also expressed in MSC but not observed in the most aggressive MIcγ model and can be identified in a subgroup of MM patients. The analysis of the MSC and EC interactions with PC revealed stage-specific interactions of relevance for angiogenesis, immunomodulation, and MM extravasation. Finally, the translational relevance of our results in humans was confirmed on MSC from newly diagnosed patients at different stages of the disease. In summary, these results indicate a remodeling of the non-hematopoietic BM microenvironment in myeloma progression, providing potential targets at the tumor-niche interface that may hold clinical significance and complement existing immunotherapies.

INTRODUCTION

Multiple myeloma (MM) is a B-cell malignancy characterized by the clonal expansion and dissemination of plasma cells (PC) in the bone marrow (BM) that is preceded by asymptomatic precursor conditions, namely monoclonal gammopathy of undetermined significance (MGUS) and smoldering multiple myeloma (SMM)[1]. Despite significant improvement in the response rate and overall survival of MM due to the introduction of novel therapies based on immunomodulatory drugs, proteasome inhibitors, anti-CD38 monoclonal antibodies, and, more recently, T-cell redirecting therapies (alternative: novel immune therapies), patients eventually relapse, and therefore, it is still considered an incurable disease[2]. Treatment of the disease at the stage of SMM in patients with a high risk of progression has been associated with an increase in progression-free survival (PFS) and may result in an increase in long-term survival and even cure of a significant proportion of patients. Understanding the molecular mechanism involved in the progression from precursor stages to symptomatic MM should be instrumental in the design of therapies directed to prevent the development of overt disease.

The BM microenvironment comprises a complex network of hematopoietic and non-hematopoietic cells, extracellular matrix components, and soluble factors. This microenvironment creates an immunosuppressive and proinflammatory milieu that supports malignant PC growth and survival[3]. Therefore, understanding the intricate interactions between myeloma cells and their surrounding microenvironment is crucial for developing effective therapies that can disrupt supportive signals and overcome drug resistance mechanisms. While most of the studies have focused on the immune component, mounting evidence suggests that endothelial cells (EC) and mesenchymal stem cells (MSC) also contribute to the survival and growth of myeloma PC through the production of cytokines and the release of extracellular vesicles[4,5]. Moreover, an enhanced inflammatory signature has been identified in MSC of patients with MM[6–8]. However, the role of the non-immune BM microenvironment in the transition from MGUS to MM remains less understood.

In the current study, we took advantage of our recently described mouse model of MM that recapitulates the principal clinical, genetic, molecular, and immunological characteristics of MM patients[9]. These models are characterized by the presence of a precursor stage equivalent to MGUS that evolves into asymptomatic MM. We performed single-cell RNA sequencing (scRNA-seq) on Fluorescent-Activated Cell Sorted (FACS) BM non-immune microenvironment cells, specifically EC and MSC, as well as PC from the same animals.

Our results identified distinct transcriptional changes between EC and MSC during the different stages of the disease. While EC are characterized by significant differences between MGUS and MM stage, changes in MSC are already identified at the MGUS stage with an inflammatory profile along with the reduction of structural functions, which is preserved in MM. Interestingly, we identified an interferon (IFN)-related myeloma signature in malignant EC, which is also expressed in MSC. Our work further characterizes interactions between microenvironment cells and malignant PC potentially involved in disease development. While interactions between EC and PC are significantly reduced during MGUS, MSC displayed an increased communication with PC compared to the EC. Finally, using MSC from patients with MGUS, SMM, and MM, we unveil similar transcriptional alterations in human MSC with an inflammatory profile underlying progression into MM.

METHODS

Mice

We used $BI_{c\gamma}$ mice (B6(Cg)-Gt (ROSA)26Sor$^{tm4(Ikbkb)Rsky}$/J mice and B6. Cg-Tg(BCL2)22Wehi/J) that recapitulate the most common changes observed in human MM preceded by an MGUS-like stage[9]. As controls, mice carrying a YFP reporter were crossed with cγ1-cre mice (B6.129 × 1-Gt (ROSA)26Sor$^{tm1(EYFP)Cos}$/J mice; The Jackson Laboratory). Moreover, we used $MI_{c\gamma}$ B6(Cg)-*Gt (ROSA)26Sor$^{tm4(Ikbkb)Rsky}$*/J and C57BL/6N-Gt(ROSA)26Sor$^{tm13(CAG-MYC,-CD2*)Rsky}$/J, a fast progression model with a less marked MGUS stage. Eight to ten-week-old mice were immunized with sheep red blood cells every 21 days for 4 months.

For each scRNA-seq experiment, a pool of five or six adult mice per group compromising control, MGUS, and MM stages was used. Mice of both sexes were used in the study. Mice were kept under specific-pathogen-free conditions in the Center for Applied Medical Research (CIMA) animal facilities at the University of Navarra. Animal experimentation was approved by the Ethical Committee of Animal Experimentation of the University of Navarra and by the Health Department of the Navarra Government.

Murine BM non-hematopoietic niche cells were isolated as previously described[10]. 25 µl from total BM were stained with PE-CD138, APC-B220, and BV421-IgM antibodies (Biolegend) to determine PC infiltration and analyzed by flow cytometry. BM non-hematopoietic cells and GFP positive (GFP^+) PC were FACS using BD FACSAria II sorter and collected in PBS 1X supplemented with 0.05% UltraPure BSA for subsequent scRNA-seq protocol. Cell viability of sorted cells was assessed using a Nexcelom Cellometer.

Human

For human studies, clinical BM aspirate samples from individuals of both sexes with newly diagnosed MGUS (n = 5), SMM (n =2), or MM (n =10) were obtained from the University of Navarra Biobank. Human BM samples from healthy adult donors (50-80 years of age) undergoing orthopedic surgery (hip or knee replacement) were harvested. All samples were collected, processed, banked, and thawed for further processing. This study was performed in accordance with the regulations of the Institutional Review Board of the University of Navarra and was conducted according to the principles of the Declaration of Helsinki. Informed consent was obtained from all patients.

After sample collection, red blood cells were lysed twice following the ratio of 45 mL of ACK lysis buffer per 5 mL of human sample. Portions of bones present in the samples were cut into small pieces, and after being crushed, the remaining fragments were collagenized with 0.3% collagenase I and dispase (5U/ml) for 15 min at 37ºC and shaking at 200 rpm. After digestion, the collagenized fractions were filtered through a 70 µm filter into a collection tube and pooled. To determine live cell concentration and viability, 10 µl of each sample was stained with acridine orange and propidium iodide (AO/PI) solution (Nexcelom) and analyzed with Cellometer K2 Image Cytometer (Nexcelom Bioscience). Cells were subsequently cryopreserved with FBS and 10% dimethyl sulfoxide (DMSO, Sigma-Aldrich) in liquid nitrogen until use.

Frozen BM samples were thawed at 37ºC in dextran-40 solution supplemented with 25% of human albumin at 20%. Cell viability of thawed cells was assessed using Nexcelom Cellometer as described above. The sample was then centrifuged and stained for 30 min on ice with the following combination of conjugated antibodies at a concentration of 1/100 except anti-Lin (3 µl/test- test $25x10^6$cells): BV510 labeled anti-Lin (including CD3, CD10, CD19, CD45, and CD64), BV421 labeled anti-CD235, BV421 labeled anti-CD45, FITC labeled anti-CD31, APC-Cy7 labeled anti-CD9, PE labeled anti-CD146 and PerCP-Cy5.5 labeled anti-CD271. For bulk RNA-sequencing (bulk RNA-seq) studies, MSC were prospectively sorted in 100 µl of Lysis/Binding Buffer (Ambion), vortexed, and stored at -80ºC until further bulk RNA-seq processing.

Single-cell RNA and Bulk RNA sequencing

The specifics related to the preparation, sequencing, and analysis of the scRNA-seq and bulk RNA-seq libraries are described in the supplemental Methods. Briefly, scRNA-seq genomic sequence reads were analyzed using the CellRanger suite against the mouse reference genome mm10 with default parameters. Next, the analysis of scRNA-seq count tables was performed using R version (v) 4.1.3 and Seurat v 4.3.0[11]. Additional information, including quality control steps, differential expression, gene set enrichment analysis (GSEA), cell-cell communication, and gene regulatory network (GRN) analysis, are fully described in the supplemental Methods.

RESULTS

Single-cell transcriptomic profiling of BM murine cells in control, MGUS, and MM

The BM niche is essential for fostering a favorable tumor microenvironment that enables the growth and survival of MM cells. Utilizing the BIcγ1 myeloma murine model[9], we characterized the influence of the stromal and endothelial BM microenvironment on the progression from MGUS to MM. This model carrying BCL2 and $IKK2^{NF\text{-}\kappa B}$ develops MGUS starting around 6 months of age and progressing to MM in 4 to 6 months. Considering that the current BIcγ1 mice are immunized, we also included YFPcγ1 mice similarly immunized as controls (**Figure 1A**). BM was harvested from control mice as well as mice with MGUS and MM (**Table S1**). Then, we performed scRNA-seq profiling on FACS-sorted BM MSC, EC (Lin^-, $TER119^-$, $CD45^-$, VDO^+, and $7AAD^-$) and myeloma PC (VDO^+, $7AAD^-$ and GFP^+) (**Figure S1**). For single-profiling BM niche cells were combined with a variable percentage of sorted PC. After quality control and preprocessing, we obtained a total of 17451 cells across all groups (2654 for control, 6122 for MGUS, and 8675 for MM). We identified

19 distinct clusters comprising MSC, EC as well as a limited number of cells from other populations of immune and non-immune BM cells (**Figure 1B).** As an additional quality control, we estimated the contribution of cells from the different stages (control, MGUS, and MM) to each cluster and cell cycle status (**Figure S2A-B**). Eight of these clusters, based on the expression of *Sdc1, Xbp1, Tnfrsf17,* and *Slamf7,* were labeled as PC (clusters 1, 2, 5, 9, 10, 11, 12, and 13, n=7924). Two clusters defined by the expression of *Hba−a1, Hba−a2, Hmgb2,* and *Car2* were labeled as erythroblasts (clusters 16, 17, n=257). One cluster, defined by the expression of *S100a8, S100a9, Fcer1g,* and *Lyz2* was labeled as neutrophils (cluster 18, n=176) (**Figure 1C; Figure S2C-D**). EC (clusters 3 and 8, n= 593) were identified by the expression of canonical genes such as *Cdh5, Cav1, Ly6c1,* and *Kdr* (**Figure 1C; Figure S2C-E**). The MSC (clusters 14 and 15, n= 593) specifically expressed mesenchymal and osteolineage (OLN)-primed markers *Cxcl12, Pdgfra, Lepr,* and *Col1a1* (**Figure 1C; Figure S2C-F**).

To better understand the roles of BM MSC and EC in myeloma progression, we first conducted a series of confirmatory analyses on both cell populations. The distribution of EC (315 control cells, 262 MGUS, and 2060 MM) was confirmed based on the expression of canonical endothelial markers such as *Cdh5* and *Pecam1* (**Figure 1D; Figure S2G-H**). Similarly, the distribution of MSC was confirmed by the expression of *Cxcl12* and *LepR* (132 control cells, 143 MGUS, and 229 MM) (**Figure 1E; Figure S2I-J**). An increase in the number of EC in the BM during MM development was verified by flow cytometry (**Figure S3**). Overall, these results validate our cell enrichment strategy for the isolation of EC and MSC within the non-hematopoietic BM compartment.

Identification of a myeloma specific IFN signature in the BM microenvironment

The observed increase in EC numbers in the context of MM emphasizes a potential connection between EC and MM progression. Delving into the composition of EC, UMAP analysis revealed a cluster of cells shared across all stages alongside a second cluster of cells ("MM2") that was nearly unique to the MM stage (**Figure 2A**). The predominance of EC from the MM stage within the "MM2" cluster suggested a central role in myeloma. The "MM2" cluster gene signature was characterized by the expression of IFN-inducible genes such as *Ifit2, Rsad2, Ifit3, Isg15, Ifi44, Ifit* and *Oasl2,* indicating an upregulation of an IFN response pathway (**Figure 2B**). Additionally, key transcriptional regulators of IFN-dependent immune responses, such as guanylate-binding proteins (GBPs) and transcription factors (TFs) of the STAT family (*Stat1* and *Stat2*), contributed to the enrichment profile as well. Over-representation analyses (ORA) confirmed the involvement of IFN-response pathways in "MM2" EC (**Figure 2C**).

To uncover the regulatory mechanisms governing the IFN-like signature, we carried out a cis-regulatory analysis to identify gene-expression-derived regulons using SCENIC[12]. This algorithm infers the differentially activated regulons, defined as a GRN co-regulated by a known transcription factor coding for a gene repressor or activator. Regulon analysis implicated *Irf7, Stat1,* and *Stat2* as master regulators significantly activated in the "MM2" EC subset (**Figure 2D; Figure S4A-B**). These TFs are widely recognized regulators of the type 1 IFN induction pathways, which have been linked to regulatory T cell immunosuppressive function observed in myeloma patients[13]. GSEA results showed that gene target members of these regulons were mainly enriched in immunity-related function terms, including type I IFN production, response to IFN, T-cell-mediated immunity, and regulation of T-cell activation (data not shown). Regulon-specific targets related to T-cell regulation, such as *Trim30d, Trim56, H2-T22, H2-T23, H2-Q6,* and *H2-Q7,* showed high expression levels in the "MM2" EC subset (**Figure S4C**).

As shown in **Figure 2E**, this signature robustly characterizes "MM2" EC in our data and highlights genes that are overexpressed in the abnormal cell subset in MM. Hence, to determine whether this IFN-like signature was unique for EC, we evaluated the score of the gene set related to "MM2" EC across other BM populations. This signature was also significantly upregulated in MSC from BIcγ1 mice with MM, suggesting a shared immunomodulatory response of the BM microenvironment to the disease (**Figure 2F**). In other cell types, including PC, neutrophils, and immature erythrocytes, among others, an IFN signature was observed at the MM stage (**Figure S4D**). As the signature is not present in cells from control or precursor stages, we concluded that this upregulation is specific to the malignant stage. Consequently, we termed this MM-IFN signature to highlight their association with IFN pathways and MM phenotype.

Interestingly, when we analyzed the MM-IFN signature in the MIcγ1 model[9], an additional model characterized by rapid MGUS-to-MM transition, we did not observe a statistically significant enrichment of the INF signature in any of the stages in either population (**Figure 2G Figure S4E**). This finding prompted us to further investigate this MM-IFN signature in humans. Using a single-cell publicly available dataset containing stromal cells from both MM patients and healthy donors[7], we uncovered an enrichment of the murine MM-IFN fingerprint in a subset of MM patients, independent of the genomic alterations (**Figure S4F-G**). Likewise, previous studies have described a similar IFN-inducible signature with highly overlapping marker genes in PC and immune microenvironment cells from certain MM patients[14,15]. This finding supports the notion that the IFN pathway could define a subgroup of patients with MM. Taken together, our data provide compelling evidence that IFN-signaling occurs not only within the non-hematopoietic BM microenvironment but also in malignant PC cells and across various immune populations within the BM. Furthermore, the identification of this specific signature at the MM stages suggest that it may be involved in the pathogenesis of a subgroup of patients with MM.

EC are characterized by a stress pre-vascular state during MGUS stage

We next analyze those EC that did not show a specific INF signature. To investigate deeper into the molecular mechanisms of myeloma progression, we performed a differential expression analysis among non-IFN EC at the different stages of the disease. A first global analysis uncovered a distinct transcriptome profile between EC from MGUS in comparison with control and MM cells (**Figure 3A**). Interestingly, EC from MGUS were characterized by overexpression of *Slpi*, *Mt1*, *Mt2*, and *Hspa5*, genes related to protein folding, endoplasmic reticulum stress and metal ion homeostasis, suggesting a stress state of EC at the onset of the disease (**Table S2; Figure 3B; Figure S5A-B**). Metallothioneins (Mts) are metal-binding proteins that play a role in several processes, including metal homeostasis, detoxification, and cell proliferation[16]. Although their connection to myeloma is less well characterized, several studies have demonstrated that metallothioneins play an essential role in tumor angiogenesis[17]. These results suggest that the upregulation of *Mt1* and *Mt2* in EC from MGUS may be involved in neovessel formation and may represent a "pre-vascular phase" in the progression to MM. Similarly, the *Hspa5* (heat shock protein 5) gene (also called *Grp78* and Binding immunoglobulin protein) favors pro-survival signaling and contributes to tumor angiogenesis[18]. Notably, during the MGUS stage, there was a significant upregulation of *Cd74*, *Tmem176a*, and *Nme2* (**Figure S5C**). While these genes are known to regulate hematopoiesis and have documented roles in various pathologic conditions, their implication in MGUS pathogenesis within the endothelium has not been previously reported[19–21].

Then, to comprehend how EC might contribute to disease progression, we performed a differential expression analysis comparing EC from MM and MGUS. Overall, 180 genes were differentially expressed in EC between both stages, including 175 upregulated and 5 downregulated genes (**Table S3; Figure 3C**). ORA revealed enrichment for biological processes involving angiogenesis, EC migration, differentiation, and epithelial cell proliferation in EC from MM, reflecting the vascular phenotype (**Figure 3D**). We also found overexpressed genes strongly related to lipid metabolism, reflecting the potential role of lipoproteins and lipids in MM[22]. Intriguingly, among the most upregulated genes in MM EC, *Sox18* was particularly interesting as this gene is critical for vascular development (**Figure S5D**). Furthermore, it has been demonstrated that *SOX18* plays a crucial role in the proliferation and migration processes of various malignant tumors, emphasizing its significance in cancer progression[23]. In addition, genes such as *Fabp4* and *Cav1* were also unregulated in EC from MM, suggesting their role in malignant transformation.

We expanded our analysis to the MIcγ1 model. Global transcriptional changes showed a similar stress transition state akin to that seen in the BIcγ1 model, marked by the upregulation of protein folding functions (**Figure S6A**). Interestingly, genes upregulated at the MGUS stage of the MIcγ1 model mirrored those elevated at the MM stage in the BIcγ1 model, supporting the rapid disease progression in the MIcγ1 model (**Figure S6B**). Likewise, we observed an increased vascular phenotype during the MGUS stage, along with the upregulation of *Anxa2*, *Anxa5*, *S100a6*, and *S100a10* in MM genes associated with a more aggressive disease[24,25] (**Figures S6C-F**).

Next, we directed our attention to the gene regulatory networks deregulated in non-IFN EC in MGUS and MM. We focus on the BIcγ1 model, as this model better mimics the slower progression observed in humans. The regulon activity analysis revealed a global decline in the activity of regulons during disease progression

(**Figure 3E; Figure S7A-B**). Xbp1 regulon displayed the highest activity in MGUS EC (**Figure 3F; Figure S7B-C**). *Xbp1* is a stress-inducible transcription factor, whose role in deregulation of the immune microenvironment of various cancers[26] has been described. *Xbp1* has also been reported to promote endothelial proliferation and angiogenesis through VEGF signaling in EC[27]. Furthermore, the overrepresentation of *Fos* regulon in EC from MGUS and MM suggested the importance of *Fos* not only in PC but also in BM EC[28] (**Figure S7C**). Interestingly, regulons from the ETS TFs family as well as *Sox18* recovered their activity in MM, which may imply the involvement of these regulons in the pathogenesis of the disease (**Figure 3F; Figure S7C**). Thus, our regulon network offers a comprehensive view of the interplay between crucial TFs and their targets that could drive the aberrant gene regulatory program of the endothelium during progression. Globally, our results support a transition during progression from MGUS to MM driven by an activation of molecular programs associated with angiogenesis and vascularization.

MSC undergo early transcriptional changes during pre-malignant MGUS that persist in overt MM

Recognizing MSC as crucial contributors to the MM microenvironment, we sought to unravel the distinct transcriptional alterations that arise during myeloma progression in non-IFN MSC. Global gene expression analysis revealed a similar transcriptional signature between MGUS and MM MSC, suggesting that the deregulation associated with the disease begins as early as the premalignant stage in the mesenchyme (**Figure 4A**). GSEA revealed a dysregulation in bone and matrix-related processes such as ossification, bone and cartilage development, extracellular matrix organization, and cell-substrate adhesion (**Figure 4B**). These results point towards an impaired osteogenic capacity of MSC during MM development, in line with previous reports in MM[5]. Besides, functional analysis revealed a downregulation of terms related to lipid metabolism and cholesterol efflux, reflecting the diminished adipogenic differentiation described in MM MSC[6,29]. Indeed, among the most downregulated genes in MGUS and MM MSC were *Col1a1*, *Col1a2*, *Bgn*, *Serpinh1*, *Sparc*, and *Clec3b* (**Figure 4B; Table S4**). Aside from these genes known to be downregulated in MSC from MM, we also found other downregulated genes involved in muscle development and regulation of smooth muscle cell proliferation, such as *Pi16*, *Myl6*, *Enpp2*, *Nupr1*, and *Shox2*, not previously implicated in MM.

As changes were already identified during the MGUS stage, we compared MSC from MGUS and control (**Table S5**). MGUS MSC exhibited a significant overexpression of oxidative phosphorylation and ATP metabolism (*Uqcrq*, *Atp5j2*, *Atp5b*, *Cox6a1*, and *Cox5a*), protein folding (*Cd74*, *Hsp90b1*, *Prdx4*, *Pdia4*, *Sh3glb1*, and *Hspe1*) and RNA processing (*Npm1*, *Prpf4b*, *Snrpd2*, *Srrm2*, and *Hnrnpa2b1*) (**Figure 4C-D**). Overexpression of *Cd74*, both in MSC and EC in MGUS stage, suggests its potential role in myeloma progression. Despite most of the transcriptional changes developed at the MGUS stage, we investigated the limited changes between MGUS and MM. Only 35 genes, of which 21 were upregulated and 14 were downregulated, showed differential expression between MM and MGUS MSC (**Figure 4E; Table S6**). GSEA analysis revealed that functions related to the immune response were the most significantly affected, resembling the inflammatory profile described in MSC from MM patients[7] (**Figure 4F-G**). Likewise, by analyzing the transcriptional differences in MSC from MIcγ1 mice, we found highly overlapping genes with the previous large-scale analysis of the BIcγ1 model (**Figure S8**), highlighting the compromised osteogenic, adipogenic, and myogenic differentiation during myeloma development.

Finally, a regulon-identification analysis was conducted to gain a better understanding of the master regulators underlying molecular regulation of MSC during each stage of the disease in BIcγ1 model (**Figure 4H; Figure S9A**). Control MSC were highly enriched in well-known TFs mediating osteochondrogenic and adipogenic differentiation, including *Sp7*, *Dlx5*, *Sox8*, *Sox9*, and *Cebpa*, as well as an enhanced activity of *Klf4* regulon, consistent with the impaired myogenic phenotype disclosed in MSC from MGUS and MM. Our analysis revealed that MGUS MSC exhibited high activity of AP-1 TFs family members (*Jun*, *Junb*, *Jund*, *Fos*, *Fosb*, *Maff*, *Atf1*, and *Atf3*). These factors have been implicated in numerous physiological processes, as well as tumorigenesis, including the development of MM[30]. Furthermore, in line with previous studies[31], Egr1 regulon showed lower activity in MSC from MM compared to MSC from MGUS. Interestingly, both MGUS and MM MSC showed high levels of Yy1 and Xbp1 regulons (**Figure S9B**). *Yy1* is known to contribute to tumorigenesis, while *Xbp1* supports MM cell growth and osteoclast formation[32,33]. On the other hand, Elk3 regulon was found to be active only in MSC from MM, suggesting a more invasive role as described in other cancers[34] (**Figure S9C**). Overall, our results suggest that MSC undergo a transcriptional shift at the stage of MGUS that persists throughout the course of the disease.

Altered crosstalk between EC and MSC with PC are potentially associated to myeloma development

The crosstalk between tumor cells and the BM microenvironment plays a vital role in the pathogenesis of malignancy. Hence, to further understand the molecular mechanism underlying niche-PC communication pathways and how they change upon the development of the disease, we analyzed cellular communication networks through ligand-receptor (L-R) analysis using LIANA[35] (**Figure 5A**). Focusing our analysis on the interactions established between EC and PC, we identified interactions present in controls as well as the different stages of the disease. Among them, EC-to-PC predicted signaling included interactions via *App* and *Cxcl12* as ligands and *Cav1*, *Itgb1*, and *Notch1* as receptors (**Figure S10A; Table S7**), whereas PC-to-EC interactions included *Gnai2* and *Tgfb1* as ligands and *Cd44*, *Itgb1*, and *Adrb2* as receptors. We next focused on specific interactions associated with malignant plasma cells. We observed a decrease in the number of interactions during the MGUS stage, followed by an increase at the myeloma stage (**Figure 5A**). Interactions, including *Fn1* as ligand and *Insr* as receptor in EC and the *Cd93* as receptor in PC, were identified only in controls, while *Apoe* as ligand in EC and *Adam9*, *C3*, and *Vegfa* as ligand in PC were only found in MM (**Figure 5B**). These results support the role of angiogenesis in myeloma progression through *Vegfa* secretion from PC, which interacts predominantly with *Kdr*, *Nrp1*, and *Nrp2* receptors in EC. Interestingly, although the later interactions are poorly characterized in MM, several reports have correlated the high expression of Nrps with poor outcomes in multiple cancer subtypes[36]. Another disease-specific interaction was the *Efna1-Epha8*, which was predicted exclusively in MM, further implicating the ephrin pathway network in disease progression. Furthermore, pathway enrichment analysis of L-R pairs revealed a significant role of Notch signaling in MM interactions, which may contribute to angiogenesis, consistent with previous research (**Figure S10B**)[37].

We next examined in detail the potential interactions between MSC and PC. Interestingly, the L-R interactome analysis of communication between the PC and the BM microenvironment revealed that most interactions are borne from MSC, and these interactions decreased along the progression of the disease (**Figure 5A; Table S8**). We first focused on interactions conserved in control and common to MGUS and MM. These interactions are mainly driven by *App*, *Fn1*, and *Cxcl12* from MSC, with *Tgfb1* being the most widely distributed ligand from PC (**Figure S10C**). Moreover, *Egfr*, *Itgb1*, and *Lrp1* were the more prevalent receptors in MSC, while *Cd44*, *Sdc1*, and *Sdc4* were the more common ones in PC. We analyzed specific interactions observed during the different disease stages. A decrease in *Itga4*-mediated communication during disease progression and specifically the loss of *Thbs1-Itga4* and *Thbs2-Itga4* interactions was observed which may be related to malignant plasma cell extravasation (**Figure 5C**). MGUS and MM PC participate in different outgoing and incoming interactions that were not predicted in healthy controls and involved *Mfge8* and *Sdc3*, respectively (**Figure 5C, Figure S10D**). *MFGE8*, in addition to controlling apoptosis, cell remodeling, and immunomodulation, has been reported to promote disease progression through the interaction with integrin αvβ3 in melanoma microenvironment[38]. Further analysis of cellular communication during the MM stage showed specific interactions related to cell motility and adhesion processes (**Figure S10D**). MM PC overexpressed *Adam9* and *Adam17*, which are predicted to bind to *Itgav* as well as *Itgb1* on MSC (**Figure 5C**). Several studies have highlighted the crucial role of ADAMs in the reorganization of the extracellular matrix, which promotes cancer egress and invasion in various types of tumors[39].

Of note, we uncovered certain L-R pairs that were common between EC and MSC with PC along the progression of the disease (**Figure 5D**). Multiple predicted interactions between MSC, EC and PC via the *Itgb5* receptor initiated during the MGUS stage. Moreover, MGUS and MM PC interacted with both MSC and EC populations by secreting *Vegfa*, indicating the importance of angiogenesis in MM. Additionally, the interactions of *C3*-mediated responses between PC and the BM microenvironment observed in MM suggest that *C3* released by PC may maintain the immunosuppressive environment of MM, as described in other types of cancer. Overall, the description of specific interactions between EC, MSC and PC during the different stages of the disease should contribute to generating new hypotheses supporting the pathogenesis of disease progression in MM.

Transcriptional dynamics of human MSC during myeloma progression

To validate some of the results generated with the mouse models, we performed bulk RNA-seq with MSC obtained from BM samples of aged matched healthy individuals, newly diagnosed MGUS (n = 5), SMM

(n =2), or MM (n =10) patients isolated by FACS (**Figure 6A, Figure S11**). The clinical characteristics of all individuals are described in **Table S9**. PCA revealed a clear distinction between human MM-MSC and Healthy Donors (HD)-MSC, with MGUS-MSC and SMM-MSC mapped in between them, showing an evolving transcriptional trajectory (**Figure 6B**).

The comparison between MGUS-MSC and HD-MSC revealed 180 DEGs (**Figure S12A; Table S10**). We found a downregulation of genes related to osteoblast differentiation and osteogenesis, such as *TNN, SPP1,* and *A2M*, that is maintained in MSC from MM patients. This is accompanied by a decrease in the Wnt signaling pathway (*WIF-1, RNF220*), which has been demonstrated to have a crucial effect on the osteogenic differentiation of MSC[40]. Furthermore, the IL-1 receptor type I was also downregulated in MSC from MGUS patients in line with previous results that have described its crucial role for MM development, promoting inflammatory osteolysis, regulating myeloma cells homing into the BM, angiogenesis, and controlling IL-6 production[41]. Besides, MSC from MGUS patients showed a significant upregulation of genes related to cell cycle, protein folding, and ubiquitination, as well as the suppression of MSC senescence (**Figure S12B**). Remarkably, MSC from MGUS patients revealed enrichment in terms related to mitochondrial activity and ATP metabolism (*MCUR1, MCUB, ATP6V0D2*) and oxidative stress (*ZNF622, HIF1A*), as previously stated in our mouse data. The deregulation of these signaling pathways in MSC from MGUS patients suggests that alterations in the tumor microenvironment play a crucial role in MM pathogenesis.

The comparison between MSC from MGUS and MM patients yielded the fewest number of DEGs, consistent with the results obtained in the mouse model where MGUS and MM MSCs showed high transcriptional similarity. Specifically, we identified 74 DEGs (41 upregulated and 33 downregulated) defining stromal changes in active MM (**Figure S12C; Table S11**). Functional enrichment analysis revealed significant increase of inflammatory function in MM-MSC, involving *IL1R1, CXCL3,* and *NFKB1,* among others (**Figure S12D**). Suggesting that a pro-inflammatory microenvironment is required for transition from premalignant stages to active myeloma. In addition, MSC from MM patients demonstrated an upregulation of certain genes associated with Epithelial-Mesenchymal Transition (EMT), such as *PHLDA1*, *FOXC2*, *PPA1*, and *CTNNB1*. This finding aligns with the potential of MSC to induce EMT through communication via extracellular vesicles, a process that has been linked with more aggressive MM and the acquisitions of drug resistance[42].

The pairwise comparison of MSC from HD *versus* MM patients confirmed the defective osteogenic differentiation and a dysfunctional immunomodulatory ability in MM-MSC (**Figure 6C, Figure S12E-F; Table S12**). Interestingly, consistent with our results in the mouse model (**Figure 4B**), human MM-MSC showed impaired myogenic differentiation, with downregulating of genes related to skeletal muscle differentiation, in comparison with HD-MSC (**Figure S12F**). In addition, GSEA revealed IFN response and TNF-α signaling via NF-KB as key pathways involved in the malignant transformation of MSC consistent with the results from our mouse model (**Figure 6D**). When we projected the previously identified IFN signature from our murine MM BM microenvironment cells, onto our human bulkRNA-seq data we observed that the IFN signature was associated with a specific subset of MM patients (**Figure 6E, Figure S12G**). Notably, this IFN enrichment was not associated with any consistent genetic alteration across patients.

Finally, we sought to determine the changes in TFs activity during myeloma progression. Several TFs activity scores in MSC from MGUS and MM patients showed an upregulation during disease progression (**Figure 6F**). Specifically, enhanced activity of TFs related to the NF-KB pathway, such as *NF-KB, NKFB1,* and *RELA*, were observed in MSC from MGUS and MM patients. Furthermore, MM-MSC exhibited increased activity of the IFN regulatory factors, *IRF1* and *IRF3*, which again emphasized the importance of the IFN signaling for the disease. In conclusion, the transcriptional reprogramming of MSC during disease progression supports a consistent pattern shared by both human patients and mouse models.

DISCUSSION

Over the last decades, our understanding of MM biology has advanced significantly, with scRNA-seq analysis driving profound insights into MM heterogeneity, tumorigenesis, and extramedullary metastasis[43–47]. An important part of this novel understanding is the evidence that the BM microenvironment contributes to the outgrowth and relapse of this neoplasia and exerts a strong supportive function for the expansion of malignant PC[7,14,48,49]. Although significant progress has been made, research has mainly concentrated on PC and their

immune microenvironment, highlighting the need for additional exploration of other components of the BM microenvironment. Here, using our BIcγ murine model[9], which mirrors MM pathogenesis, we provide a comprehensive overview of the transcriptional deregulation within the BM EC and MSC during the transition from healthy BM to MGUS and eventually MM. Our single-cell transcriptomic analysis has revealed the temporal remodeling of the BM microenvironment during MM development detailing the longitudinal transcriptional alterations and the dynamic interplay between PC, EC, and MSC. Moreover, using bulkRNA-seq of human MSC from MGUS, SMM, and MM patients, we observe a consistency of transcriptional reprogramming of these cells across human patients and mouse models.

A fundamental finding of our study is the identification of a myeloma-specific IFN signature that affects several cellular components of the BM microenvironment. Notably, we observed that this MM-IFN signature is not exclusive to EC, but also extends to MSC, suggesting a shared response of the BM microenvironment during myeloma progression. While the IFN-related signature has previously been reported in PC and the immune environment[14,15,50], our data reveal that, in fact, non-hematopoietic cells also exhibit the IFN fingerprint. This IFN-related signature is marked by the upregulation of IFN-inducible genes and involved master regulators such as *Irf7*, *Stat1*, and *Stat2*. Previous studies highlighted *STAT3* as an oncogenic driver in MM and reported the role of *STAT1* in promoting MM cell migration and BM homing[51]. The heightened correlation between Stat signaling and the IFN in the EC and MSC from MM expands the emerging tumor-promoting roles described for Stat1 and Stat2 pathways.

This IFN-inducible signature not only suggests an active response pathway but also unveils a new potential role in immune modulation within the non-immune BM microenvironment. We speculate that the reprogramming of EC and MSC into IFN-inducible signaling may contribute to the remodeling of immune functions, potentially promoting T-cell exhaustion under inflammatory conditions[13]. This association hints at a complex interplay between the immune system and the BM microenvironment in myeloma, suggesting the immunomodulatory potential of EC and MSC[52]. Extending our observations to human MM data, we reinforce the relevance and applicability of the identified MM-IFN signature to the clinical setting. The enrichment of the murine IFN fingerprint in MSC from a subset of MM patients, along with its correlation with previous studies[14,15], may help to define a narrower patient group within the MM heterogeneity. This role of IFN signaling shaping the BM environment during myeloma progression, could be particularly relevant in patients with a more inflammatory component.

The examination of the molecular mechanisms governing myeloma progression within non-IFN EC identified transcriptional and regulatory changes during MGUS with the upregulation of genes related to protein folding and metal ion homeostasis, such as heat shock proteins and metallothioneins. The upregulation of genes such as *Slpi*, *Mt1*, *Mt2*, and *Hspa5*, known for their roles in tumor angiogenesis and pro-survival signaling[17,53] may serve as promising early indicators of myeloma development in EC. Remarkably, our analysis unveils unexpected upregulation of genes like *Cd74*, *Tmem176a*, and *Nme2* in MGUS EC, indicating their potential involvement in MM pathogenesis, although their precise roles require further elucidation. Comparing the transcriptional profiles of MGUS and MM EC reveals dynamic changes associated with disease progression, including alterations in angiogenesis, endothelial migration, and lipid metabolism, reflecting the vascular phenotype and metabolic alterations characteristic of MM EC. The upregulation of *Sox18*, a key regulator of vasculature development and cancer progression[23], in MM EC highlights its targeting potential.

Unlike EC, transcriptional changes in MSC were already present during the MGUS stage. These changes mirror those seen in advanced MM, including impairment in osteogenic and adipogenic differentiation, as previously reported in myeloma[5,6]. Thereby, MGUS MSC may exhibit a reshaping of their differentiation capacity and metabolism to support the growth of MM cells from the early stages of the disease[54]. Despite these similarities between MGUS and MM-MSC, comparative gene expression analysis showed additional changes in MSC from MM. In a recent study, De Jong et al. identified a sub-population of MSC within the microenvironment of MM patients, exhibiting an inflammatory transcriptional signature[7]. Building upon these findings, we observed the enrichment of cytokines, TNFα, and NF-κB signaling pathways, supporting the contribution of MM MSC to the pro-inflammatory tumor microenvironment. Additionally, the upregulation of type 1 IFN signaling pathways in MM MSC reinforces the essential role of IFN in the progression of the disease. The selective regulation of MGUS MSC by Egr1 and AP-1 TF[30,31], as well as the involvement of the

Elk3 regulon in maintaining an invasive phenotype in MM MSCs, highlight the complex transcriptional networks underlying disease pathogenesis, making them potential biomarkers and therapeutic targets for MM treatment.

Understanding the intricate molecular crosstalk between the BM microenvironment cells and malignant PC is crucial for unraveling the mechanisms underlying tumor progression. Our cell communication analysis identified a tapestry of interactions targeting both myeloma cells and their surrounding microenvironment that shapes the landscape from MGUS to MM. This L-R analysis revealed altered crosstalk between EC, MSC cells and PC, primarily orchestrated by MSC. To our knowledge, this study represents the first investigation into the predicted interactions between endothelial and mesenchymal resident cells and neoplastic PC along the continuum of MM disease progression. Analysis of interactions between EC and PC uncovered a communication decline in the MGUS stage that was restored in MM, highlighting the evolving relationship between them during myeloma progression. These interactions, especially those involving *Vegfa* secretion from PC and its interactions with *Kdr*, *Nrp1*, and *Nrp2* endothelial receptors, emphasize the importance of angiogenesis as a hallmark of MM development. Additionally, identifying specific interactions exclusively in MM, such as *Efna1-Epha8*, implicates the ephrin pathway network in disease development. The involvement of this axis in the pathogenesis of other cancers, such as glioblastoma, melanoma, or breast cancer, has been described[55]. Remarkably, predicted interactions between MSC and PC were associated with adhesion, extracellular matrix organization, and migration pathway networks, suggesting their crucial role in promoting MM cell extravasation, emphasizing the substantial role of MSC-PC crosstalk as a potential contributor to the dissemination of the disease.

Challenges associated with the scarcity of BM stromal and EC hinder scRNA seq studies in humans. Our bulk RNA-seq results showed that MSC from human patients exhibit compromised differentiation capacities, which is also apparent in the early stages of disease progression, in line with our findings in mice. Similarly, human MSC also experiences a metabolic swift in MGUS stage associated with increased protein folding ability. Human MM-MSC exhibit higher expression of angiogenesis and inflammation-related genes This inflammatory microenvironment could aid in the immune evasion of MM by suppressing T cells, which could be enhanced by the MM-MSC overexpressing genes such as *LGALS9* or *FADD*[56,57]. On the contrary, some genes related to extracellular matrix organization such as *SDC2*, *SDC4*, *MMP14* or *LAMC1* that appear to be upregulated in human MM-MSC, are downregulated in murine MM MSC. This discrepancy between both species could be explained by the heterogeneity of MM patients and their different clinical characteristics. Notably, all the mentioned genes are linked to patients with poor outcomes, which might not align with the characteristics of our mouse BIcγ1 model.

In summary, the utilization of the BIcγ1 myeloma murine model, which recapitulates the progression from MGUS to full-blown MM, coupled with the utilization of scRNA-seq and the bioinformatic toolkit associated (e.g., GRN and cellular interactome among others), enable a comprehensive dissection of the BM microenvironment. The myeloma-specific IFN signature, the distinct transition stress state in MGUS EC, the early transcriptional shifts in MSC, and the evolving cellular communication networks collectively reinforce the role of the BM microenvironment in MM development from premalignant stages. Additionally, the validation of our murine model findings in human patients strengthens the translational relevance of our study and emphasizes the importance of further investigation into the molecular mechanisms underlying MM progression. Overall, these results suggest that changes in the non-immune fraction of the BM microenvironment could create a more permissive microenvironment that favors the development of MM from premalignant stages.

ACKNOWLEDGEMENTS
This work was supported by the Instituto de Salud Carlos III and co-financed by ERDF A way of making Europe (PI20/01308, PI23/00516); CIBERONC (CB16/12/00489), RICORS TERAV (RD21/0017/0009); Departamento de Industria Gobierno de Navarra (AGATA 0011-1411-2020-000010/0011-1411-2020-000011) and Departamento de Salud Gobierno de Navarra; the Cancer Research UK [C355/A26819]; FC AECC and AIRC under the Accelerator Award Program; The International Myeloma Foundation (Brian van Novis) and The Paula and Rodger Riney Foundation to FP. The study was also supported by The Spanish Government, through project PID2019-111192GA-I00 (MICINN) to DGC. IC was supported by Marie Curie grant (H2020- MSCA-IF-837491) from European Commission. ICA was supported by AECC predoctoral fellowship (PRDNA19006CENZ). MC was supported by FPU fellowship (FPU22/03283) from Ministerio de Ciencia, Innovación y Universidades.

We would like to thank the staff of the flow cytometry core, the advanced genomic lab, and the animal facility at CIMA Universidad de Navarra for their invaluable technical and intellectual assistance. We also acknowledge Hospital Reina Sofía de Tudela, Hospital Universitario de Navarra, the Biobank of the University of Navarra, and Goretti Ariz for the provision of BM samples and their collaboration. We are particularly grateful to the patients and healthy donors for their participation in this study.

AUTHORSHIP CONTRIBUTIONS
I.C. and M.C. processed murine and human BM samples. I.C. conceptualized the study, analyzed and interpreted the scRNA-seq experiments data, and wrote the paper; M.C. analyzed and interpreted the bulk RNA-seq experiments data; A.B. performed the cell-cell computational analysis; M.L. and J.A.M.C. designed and provided the mice models; A.V., P.S.M., and P.A.R. performed the scRNA-seq and bulk RNA-seq experiments. D.A. and A.L. performed the FACS sorting. M.M.B., D.Q.A., I.S.G., and J.R. provided the BM samples from healthy adult donors; P.R.O. and L.E.T.A provided the BM samples from MGUS, SMM, and MM patients; D.G.C., with help from M.H., I.M.S, supervised the computational work; I.A.C. and B.S. designed the research experiments; F.P., D.G.C. and I.A.C conceived and directed the research project.
All authors actively participated in the discussions underlying this manuscript. I.C., M.C., I.A.C., D.G.C., and F.P. discussed the results and wrote the final manuscript. All authors contributed to, read, and approved the final manuscript.

DISCLOSURE OF CONFLICTS OF INTEREST
The authors declare no competing interests.

REFERENCES

1. Kumar SK, Rajkumar V, Kyle RA, et al. Multiple myeloma. *Nat Rev Dis Primers*. 2017;3(1):17046.
2. Mateos M-V, Nooka AK, Larson SM. Moving Toward a Cure for Myeloma. *American Society of Clinical Oncology Educational Book*. 2022;(42):643–654.
3. Lomas OC, Tahri S, Ghobrial IM. The microenvironment in myeloma. *Curr Opin Oncol*. 2020;32(2):170–175.
4. García-Ortiz A, Rodríguez-García Y, Encinas J, et al. The Role of Tumor Microenvironment in Multiple Myeloma Development and Progression. *Cancers (Basel)*. 2021;13(2):217.
5. Maiso P, Mogollón P, Ocio EM, Garayoa M. Bone Marrow Mesenchymal Stromal Cells in Multiple Myeloma: Their Role as Active Contributors to Myeloma Progression. *Cancers 2021, Vol. 13, Page 2542*. 2021;13(11):2542.
6. Alameda D, Saez B, Lara-Astiaso D, et al. Characterization of freshly isolated bone marrow mesenchymal stromal cells from healthy donors and patients with multiple myeloma: transcriptional modulation of the microenvironment. *Haematologica*. 2020;105(9):e470.
7. de Jong MME, Kellermayer Z, Papazian N, et al. The multiple myeloma microenvironment is defined by an inflammatory stromal cell landscape. *Nature Immunology 2021 22:6*. 2021;22(6):769–780.
8. de Jong MME, Fokkema C, Papazian N, et al. An IL-1β-driven neutrophil–stromal cell axis fosters a BAFF-rich protumor microenvironment in individuals with multiple myeloma. *Nature Immunology 2024*. 2024;1–14.
9. Larrayoz M, Garcia-Barchino MJ, Celay J, et al. Preclinical models for prediction of immunotherapy outcomes and immune evasion mechanisms in genetically heterogeneous multiple myeloma. *Nat Med*. 2023;29(3):632–645.
10. Ye J, Calvo IA, Cenzano I, et al. Deconvolution of the hematopoietic stem cell microenvironment reveals a high degree of specialization and conservation. *iScience*. 2022;25(5):104225.
11. Stuart T, Butler A, Hoffman P, et al. Comprehensive Integration of Single-Cell Data. *Cell*. 2019;177(7):1888-1902.e21.
12. Aibar S, González-Blas CB, Moerman T, et al. SCENIC: Single-cell regulatory network inference and clustering. *Nat Methods*. 2017;14(11):1083.
13. Sumida TS, Dulberg S, Schupp JC, et al. Type I interferon transcriptional network regulates expression of coinhibitory receptors in human T cells. *Nature Immunology 2022 23:4*. 2022;23(4):632–642.
14. Zavidij O, Haradhvala NJ, Mouhieddine TH, et al. Single-cell RNA sequencing reveals compromised immune microenvironment in precursor stages of multiple myeloma. *Nature Cancer 2020 1:5*. 2020;1(5):493–506.
15. Boiarsky R, Haradhvala NJ, Alberge JB, et al. Single cell characterization of myeloma and its precursor conditions reveals transcriptional signatures of early tumorigenesis. *Nature Communications 2022 13:1*. 2022;13(1):1–15.
16. Bensellam M, Laybutt DR, Jonas JC. Emerging Roles of Metallothioneins in Beta Cell Pathophysiology: Beyond and above Metal Homeostasis and Antioxidant Response. *Biology 2021, Vol. 10, Page 176*. 2021;10(3):176.
17. Zhu Y, Chang S, Liu J, Wang B. Identification of a novel cuproptosis-related gene signature for multiple myeloma diagnosis. *Immun Inflamm Dis*. 2023;11(11):e1058.
18. Binet F, Sapieha P. ER Stress and Angiogenesis. *Cell Metab*. 2015;22(4):560–575.
19. Le Hiress M, Tu L, Ricard N, et al. Proinflammatory signature of the dysfunctional endothelium in pulmonary hypertension role of the macrophage migration inhibitory factor/CD74 complex. *Am J Respir Crit Care Med*. 2015;192(8):983–997.
20. Ye C, Ren S, Sadula A, et al. The expression characteristics of transmembrane protein genes in pancreatic ductal adenocarcinoma through comprehensive analysis of bulk and single-cell RNA sequence. *Front Oncol*. 2023;13:1047377.
21. Bai W, Wang H, Bai H. Identification of Candidate Genes and Therapeutic Agents for Light Chain Amyloidosis Based on Bioinformatics Approach. *Pharmgenomics Pers Med*. 2019;12:387.
22. Lazaris V, Hatziri A, Symeonidis A, Kypreos KE. The Lipoprotein Transport System in the Pathogenesis of Multiple Myeloma: Advances and Challenges. *Front Oncol*. 2021;11:638288.
23. Olbromski M, Podhorska-Okołów M, Dzięgiel P. Role of the SOX18 protein in neoplastic processes. *Oncol Lett*. 2018;16(2):1383.
24. Ismail NH, Mussa A, Al-Khreisat MJ, et al. Proteomic Alteration in the Progression of Multiple Myeloma: A Comprehensive Review. *Diagnostics 2023, Vol. 13, Page 2328*. 2023;13(14):2328.
25. Liu M, Wang Y, Miettinen JJ, et al. S100 Calcium Binding Protein Family Members Associate With Poor Patient Outcome and Response to Proteasome Inhibition in Multiple Myeloma. *Front Cell Dev Biol*. 2021;9:.
26. Zhong Z, Wang J, Han Q, et al. XBP1 impacts lung adenocarcinoma progression by promoting plasma cell adaptation to the tumor microenvironment. *Front Genet*. 2022;13:969536.
27. Yang J, Xu J, Danniel M, et al. The interaction between XBP1 and eNOS contributes to endothelial cell migration. *Exp Cell Res*. 2018;363(2):262–270.

28. Jin Y, Chen K, De Paepe A, et al. Active enhancer and chromatin accessibility landscapes chart the regulatory network of primary multiple myeloma. *Blood*. 2018;131(19):2138–2150.
29. Fairfield H, Costa S, Falank C, et al. Multiple Myeloma Cells Alter Adipogenesis, Increase Senescence-Related and Inflammatory Gene Transcript Expression, and Alter Metabolism in Preadipocytes. *Front Oncol*. 2021;10:1.
30. Fan F, Podar K. The Role of AP-1 Transcription Factors in Plasma Cell Biology and Multiple Myeloma Pathophysiology. *Cancers (Basel)*. 2021;13(10):.
31. Chen L, Wang S, Zhou Y, et al. Identification of early growth response protein 1 (EGR-1) as a novel target for JUN-induced apoptosis in multiple myeloma. *Blood*. 2010;115(1):61–70.
32. Huerta-Yepez S, Liu H, Baritaki S, et al. Overexpression of Yin Yang 1 in bone marrow-derived human multiple myeloma and its clinical significance. *Int J Oncol*. 2014;45(3):1184–1192.
33. Xu G, Liu K, Anderson J, et al. Expression of XBP1s in bone marrow stromal cells is critical for myeloma cell growth and osteoclast formation. *Blood*. 2012;119(18):4205.
34. Lee M, Cho HJ, Park KS, Jung HY. ELK3 Controls Gastric Cancer Cell Migration and Invasion by Regulating ECM Remodeling-Related Genes. *Int J Mol Sci*. 2022;23(7):.
35. Dimitrov D, Türei D, Garrido-Rodriguez M, et al. Comparison of methods and resources for cell-cell communication inference from single-cell RNA-Seq data. *Nature Communications 2022 13:1*. 2022;13(1):1–13.
36. Benwell CJ, Johnson RT, Taylor JAGE, Price CA, Robinson SD. Endothelial VEGFR Coreceptors Neuropilin-1 and Neuropilin-2 Are Essential for Tumor Angiogenesis. *Cancer Research Communications*. 2022;2(12):1626–1640.
37. Saltarella I, Frassanito MA, Lamanuzzi A, et al. Homotypic and Heterotypic Activation of the Notch Pathway in Multiple Myeloma-Enhanced Angiogenesis: A Novel Therapeutic Target? *Neoplasia*. 2019;21(1):93–105.
38. Jinushi M, Nakazaki Y, Carrasco DR, et al. Milk fat globule EGF-8 promotes melanoma progression through coordinated Akt and twist signaling in the tumor microenvironment. *Cancer Res*. 2008;68(21):8889–8898.
39. Fan X, Wang Y, Zhang C, et al. ADAM9 Expression Is Associate with Glioma Tumor Grade and Histological Type, and Acts as a Prognostic Factor in Lower-Grade Gliomas. *Int J Mol Sci*. 2016;17(9):.
40. Kim JH, Liu X, Wang J, et al. Wnt signaling in bone formation and its therapeutic potential for bone diseases. *Ther Adv Musculoskelet Dis*. 2013;5(1):13–31.
41. Dinarello CA. Interleukin-1 in the pathogenesis and treatment of inflammatory diseases. *Blood*. 2011;117(14):3720–3732.
42. Kletukhina S, Neustroeva O, James V, Rizvanov A, Gomzikova M. Role of Mesenchymal Stem Cell-Derived Extracellular Vesicles in Epithelial–Mesenchymal Transition. *Int J Mol Sci*. 2019;20(19):4813.
43. Cohen YC, Zada M, Wang SY, et al. Identification of resistance pathways and therapeutic targets in relapsed multiple myeloma patients through single-cell sequencing. *Nature Medicine 2021 27:3*. 2021;27(3):491–503.
44. Ledergor G, Weiner A, Zada M, et al. Single cell dissection of plasma cell heterogeneity in symptomatic and asymptomatic myeloma. *Nature Medicine 2018 24:12*. 2018;24(12):1867–1876.
45. Dutta AK, Alberge JB, Sklavenitis-Pistofidis R, et al. Single-cell profiling of tumour evolution in multiple myeloma — opportunities for precision medicine. *Nature Reviews Clinical Oncology 2022 19:4*. 2022;19(4):223–236.
46. Samur MK, Szalat R, Munshi NC. Single-cell profiling in multiple myeloma: insights, problems, and promises. *Blood*. 2023;142(4):313–324.
47. Tirier SM, Mallm JP, Steiger S, et al. Subclone-specific microenvironmental impact and drug response in refractory multiple myeloma revealed by single-cell transcriptomics. *Nature Communications 2021 12:1*. 2021;12(1):1–16.
48. John L, Poos AM, Brobeil A, et al. Resolving the spatial architecture of myeloma and its microenvironment at the single-cell level. *Nature Communications 2023 14:1*. 2023;14(1):1–17.
49. Sharma NS, Choudhary B. Good Cop, Bad Cop: Profiling the Immune Landscape in Multiple Myeloma. *Biomolecules*. 2023;13(11):.
50. Kellermayer Z, Tahri S, Jong MME de, et al. Immune-mediated tumor control in the 5TGM1 transfer model of multiple myeloma. *bioRxiv*. 2023;2023.01.18.524505.
51. Chong PSY, Chng WJ, de Mel S. STAT3: A Promising Therapeutic Target in Multiple Myeloma. *Cancers (Basel)*. 2019;11(5):.
52. Hazrati A, Malekpour K, Khorramdelazad H, Rajaei S, Hashemi SM. Therapeutic and immunomodulatory potentials of mesenchymal stromal/stem cells and immune checkpoints related molecules. *Biomarker Research 2024 12:1*. 2024;12(1):1–26.
53. Si M, Lang J. The roles of metallothioneins in carcinogenesis. *J Hematol Oncol*. 2018;11(1):.
54. Zhan X, Yu W, Franqui-Machin R, et al. Alteration of mitochondrial biogenesis promotes disease progression in multiple myeloma. *Oncotarget*. 2017;8(67):111213–111224.
55. Pergaris A, Danas E, Goutas D, et al. The Clinical Impact of the EPH/Ephrin System in Cancer: Unwinding the Thread. *Int J Mol Sci*. 2021;22(16):.

56. Akiyama K, Chen C, Wang D, et al. Mesenchymal-Stem-Cell-Induced Immunoregulation Involves FAS-Ligand-/FAS-Mediated T Cell Apoptosis. *Cell Stem Cell*. 2012;10(5):544–555.
57. Kim S, Lee H-J, Jeon M-S, Yi T, Song SU. Galectin-9 is Involved in Immunosuppression Mediated by Human Bone Marrow-derived Clonal Mesenchymal Stem Cells. *Immune Netw*. 2015;15(5):241.

FIGURE LEGENDS

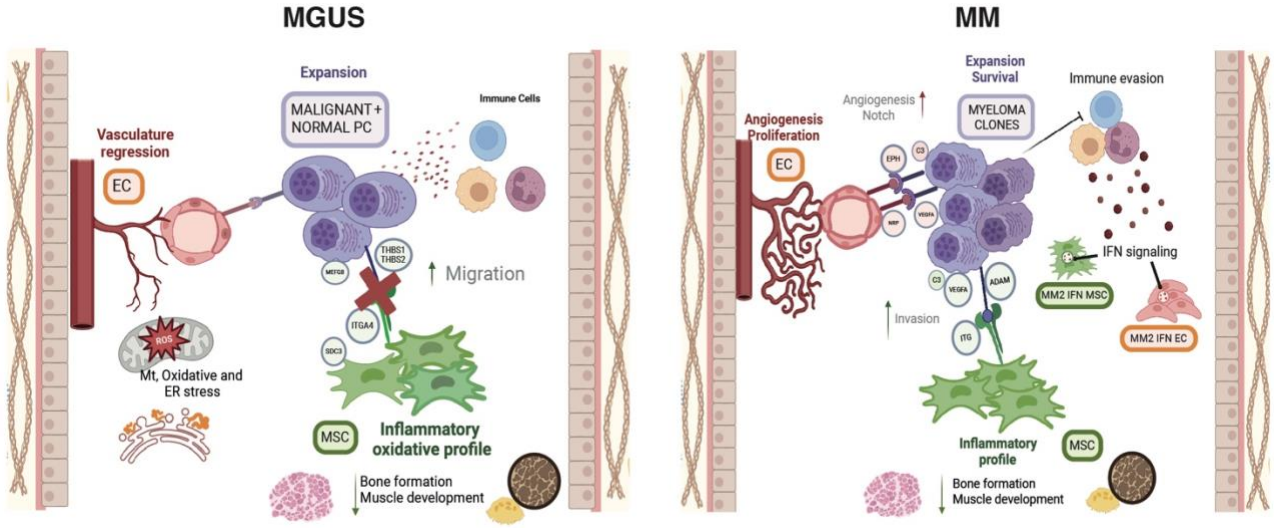

Graphical Abstract.

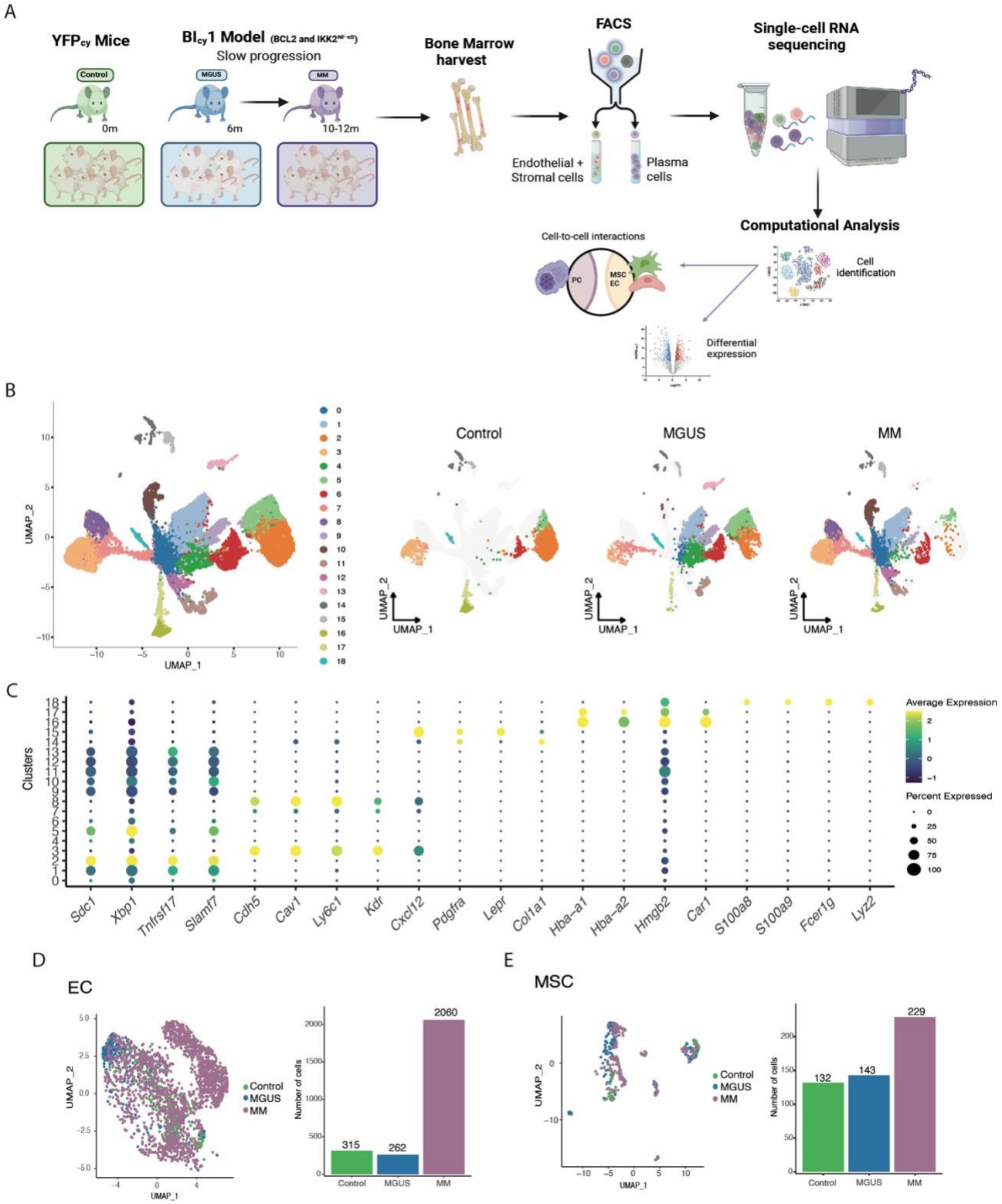

Figure 1. Single-cell transcriptomic profiling of BM murine cells in control, MGUS, and MM. (A) Experiment overview. Schematic view of control and BIcγ1 mice and experimental workflow for the isolation and scRNA-seq analysis of PC and BM MSC and EC cells. (B) UMAP representation of murine BM microenvironment control, MGUS, and MM cells colored by cell clustering after merging samples. Right panel: Original UMAP split into control, MGUS, and MM datasets. (C) Dot plot of canonical markers used to define PC, EC, MSC, erythrocyte precursors, and neutrophils. The dot size reflects the percentage of cells within the cluster expressing each gene, and the color represents the average expression level. (D-E) Left panel: UMAP projection showing the distribution of control, MGUS, and MM cells for EC (D) and MSC (E) Right panel: Bar plot depicting the total number of cells per stage for EC (D) and MSC (E).

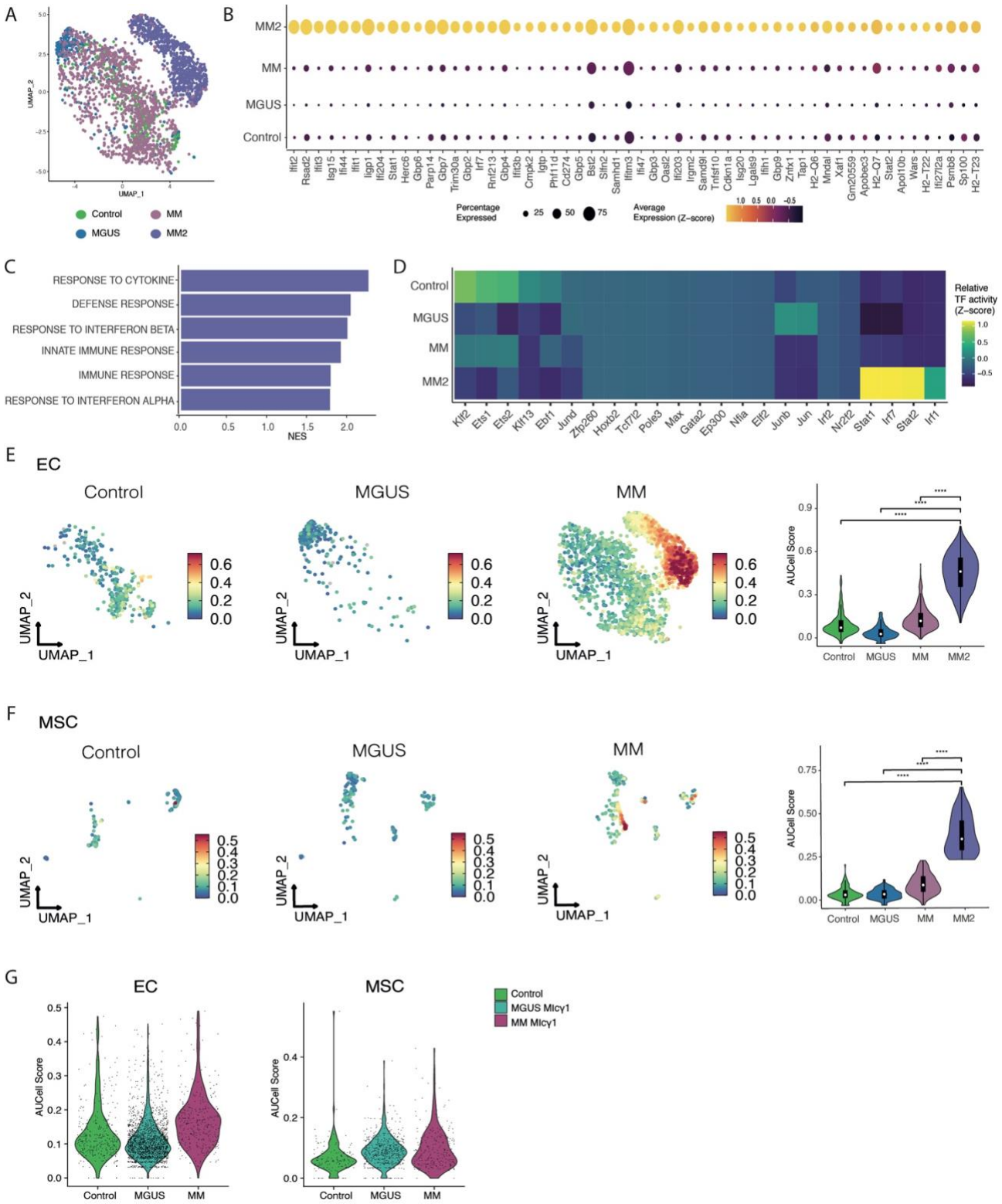

Figure 2. Identification of a myeloma specific IFN signature in the BM microenvironment. (A) UMAP dimension reduction of EC revealing a transcriptionally distinct population in MM. (B) Dot plot visualization of the markers defining EC MM2 cluster. Average gene expression is shown by color intensity, and the percentage of cells expressing each gene is shown by size. (C) Bar charts of enriched Gene Ontology (GO) terms from GSEA (FDR < 0.05) computed using MM2 cluster markers. The horizontal axis represents the normalized enrichment scores (NES). (D) Heatmap representing z-scaled mean regulon activity score of inferred top specific regulons for each stage. (E) Left panel: UMAP plot illustrating the distribution of the IFN-

related signature in EC across control, MGUS, and MM. Right panel: Violin plots showing AUC-score for IFN-related signature within EC in control, MGUS, MM and MM2 cells. (F) Left panel: UMAP plot illustrating the distribution of the IFN-related signature in MSC across control, MGUS, and MM. Right panel: Violin plots showing AUC-score for IFN-related signature within MSC in control, MGUS, MM and MM2 cells. (G) Violin plots of the AUC-score for IFN-related signature within EC (left panel) and MSC (right panel) in control, MGUS, and MM cells from the MIcγ1model.

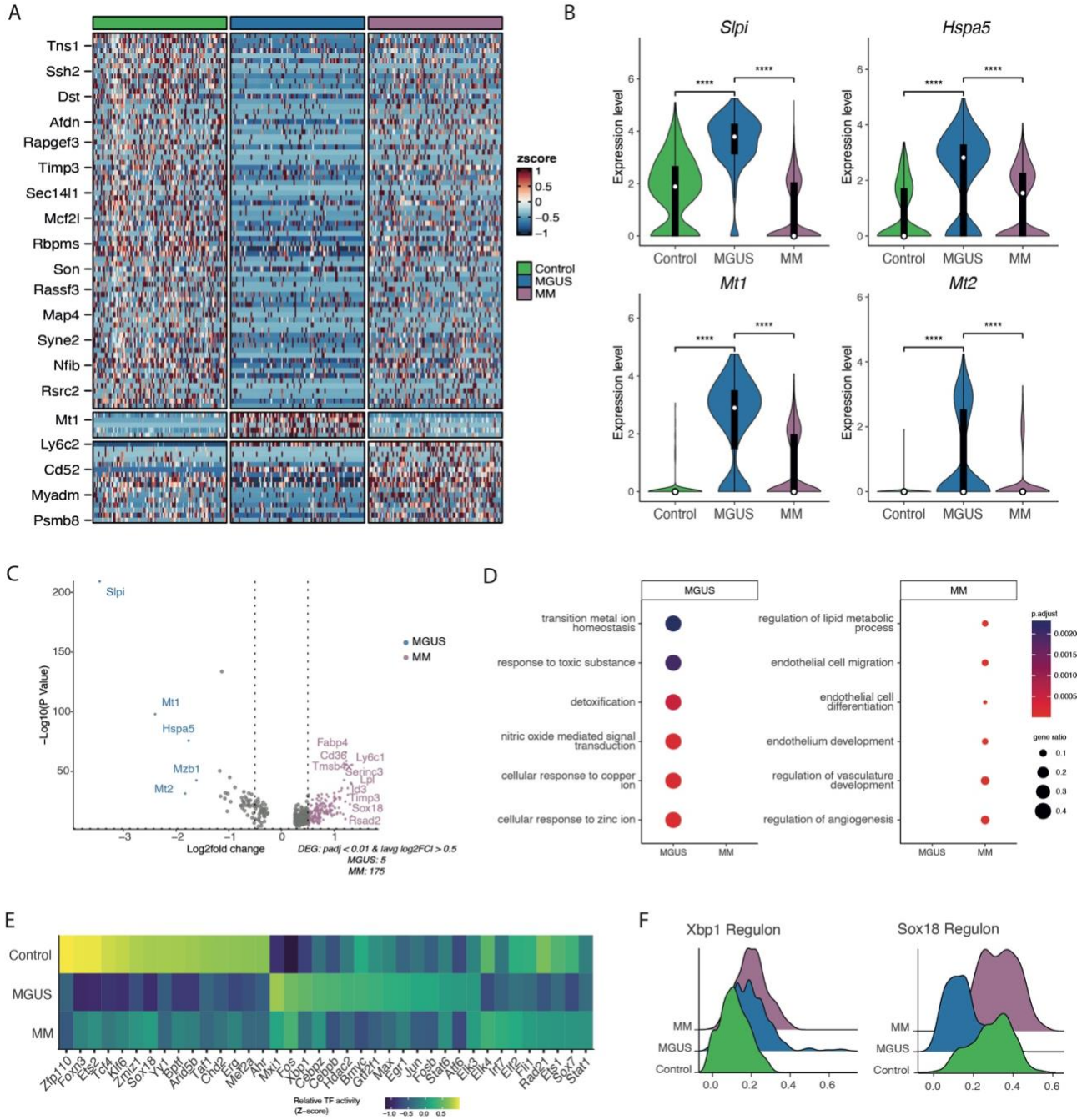

Figure 3. EC are characterized by a stress pre-vascular state during MGUS stage. (A) Heatmap of the DEG between control, MGUS, and MM cells. Color represents the z-score scaled expression values. (B) Violin plots showing the distribution of expression of genes upregulated in MGUS EC. (C) Volcano plot of the DEGs in MGUS vs. MM EC. The y-axis represents the -log10(p-value) and the x-axis represents the log2(fold change). The dot's color denotes the disease stage for which that DEG was detected, with grey dots representing non-significant genes. (D) Significant terms derived from ORA between EC from MGUS and MM. (E)

Heatmap representing z-scaled mean regulon activity score of inferred top specific regulons for EC in each stage. (F) Density plots showing the activity score of Xbp1 and Sox18 regulons in EC.

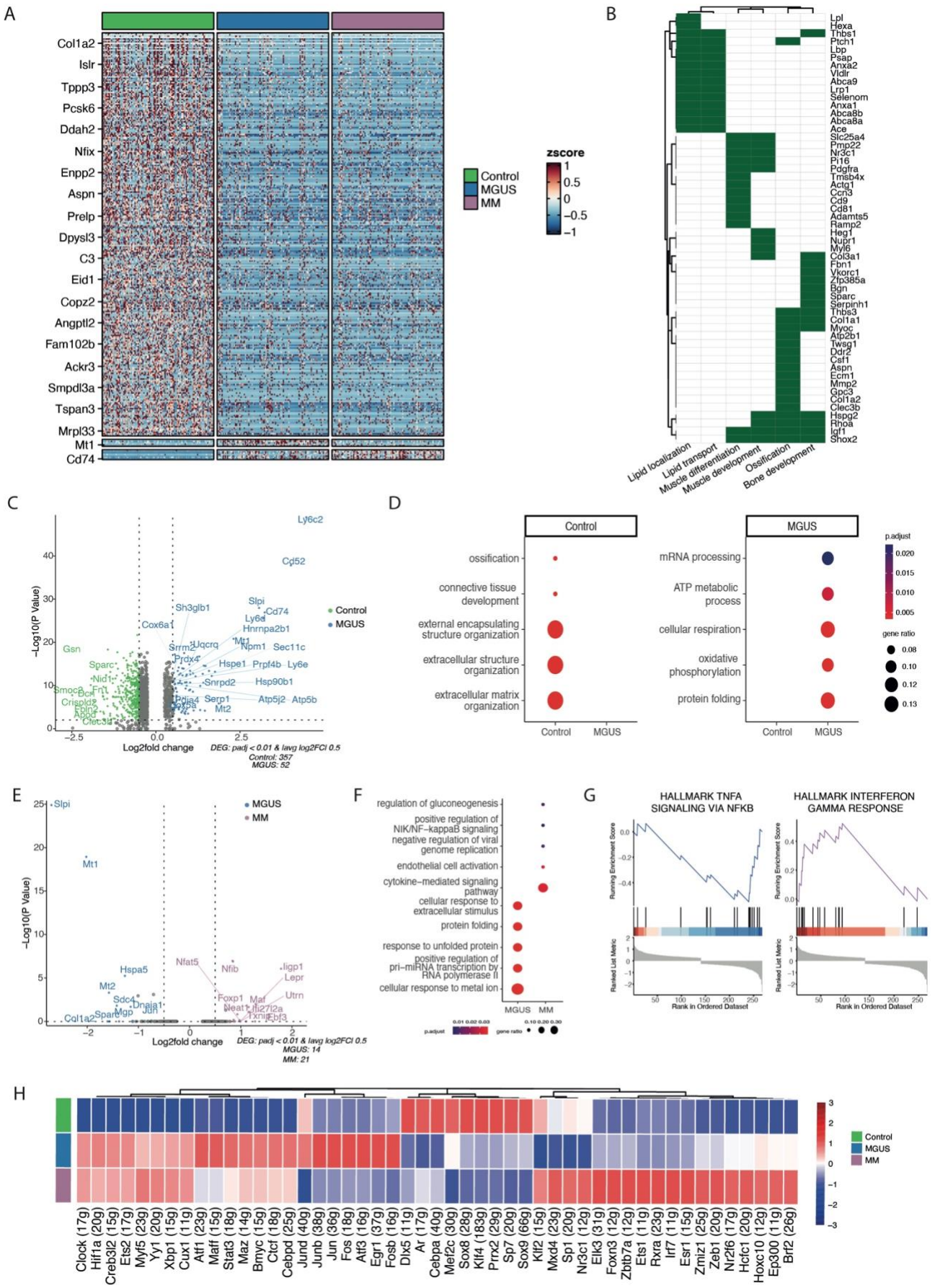

Figure 4. MSC undergo early transcriptional changes during pre-malignant MGUS that persist in overt MM. (A) Heatmap depicting DEG between MSC in control, MGUS, and MM. Color represents the z-score

scaled expression values. (B) Heatmap of significantly enriched GO terms in control MSC with the associated genes. The green color represents the presence of the gene in each GO term. (C) Volcano plot of the DEGs from the comparison between MSC from control and MGUS. The y-axis represents the -log10(p-value), and the x-axis represents the log2(fold change) of the gene. The dot's color denotes the disease stage for which that DEG was detected, with grey dots representing non-significant genes. (D) Significant terms derived from ORA of MSC from control vs MGUS. (E) Volcano plot of the DEGs in MSC from MGUS vs. MM. (F) ORA between MSC from MGUS and MM. (G) GSEA plots for the gene sets 'TNFα signaling via NFκB' (left panel) and 'Interferon gamma response' (right panel) in MGUS vs MM MSC. (H) Heatmap of mean regulon activity score of significantly enriched regulons in each stage. The color scale represents the z-score of the activity scaled by row.

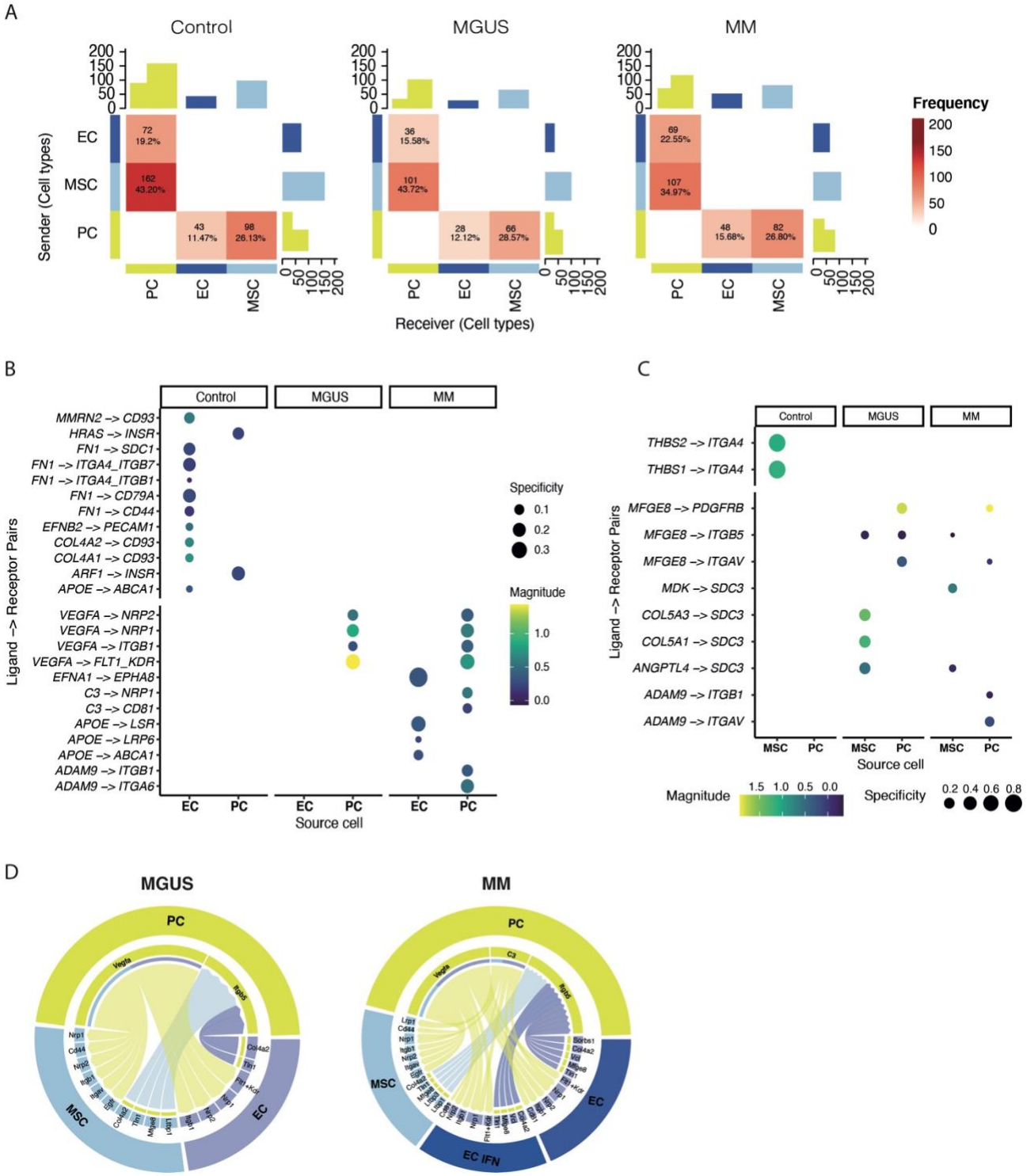

Figure 5. Altered crosstalk between EC and MSC with PC are potentially associated to myeloma development. (A) Heatmap showing the number of predicted cellular interactions between EC, MSC and PC. Block sizes and colors are proportional to the number of ligand-receptor pairs. (B-C) Dot plots of representative ligand-receptor interactions between PC and EC (B) or MSC (C) during disease progression. Dot size and color indicate the specificity and the strength of the interaction, respectively. (D) Chord diagram showing shared relevant signaling network between EC, MSC and PC in the MGUS and MM stages. Colors and width represent signal senders and strength, respectively.

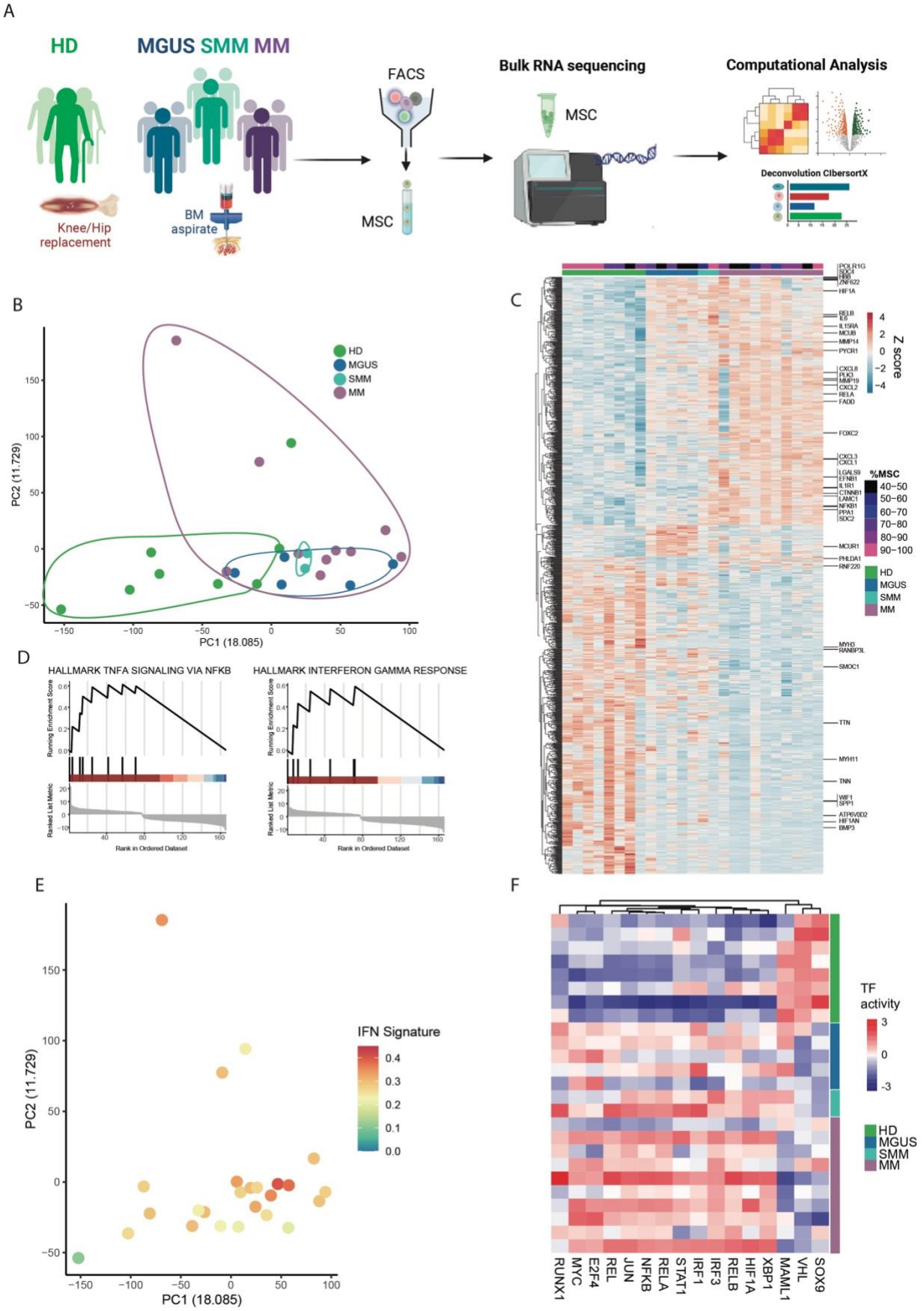

Figure 6. Transcriptional dynamics of human MSC during myeloma progression. (A) Experimental

workflow used for the isolation and bulk RNA-seq analysis of human BM MSC. (B) PCA of MSC expression profiles shows clustering by disease stage. The color of the dots represents disease stages. (C) Summary heatmap showing the expression profiles across samples of DEGs identified in each pairwise comparison along disease progression. (D) GSEA plots for the gene sets 'TNFα signaling via NFκB' (left panel) and 'Interferon gamma response' (right panel) in the comparison between HD and MM patients. (E) PCA plot representing the IFN signature score per patient. (F) Heatmap representing the variation of TF activity score across samples.

SUPPLEMENTARY MATERIAL

Supplemental Methods

Supplemental Figures

- Supplemental Figure 1: Cell sorting strategy for murine scRNA-seq of BM niche cells.
- Supplemental Figure 2: scRNA-seq Analysis of murine BM niche cells.
- Supplemental Figure 3: Flow cytometric quantification of the percentage of EC, MSC, and OB in control, MGUS, and MM BIcγ1 mice.
- Supplemental Figure 4: Additional information on the MM IFN-related signature and validation in the MIcγ1 model and scRNA-seq human data.
- Supplemental Figure 5: Additional visualizations of transcriptional differences detected between control, MGUS, and MM EC excluding MM IFN cells.
- Supplemental Figure 6: Transcriptional remodeling of EC during myeloma progression in the MIcγ1 model.
- Supplemental Figure 7: Gene regulatory network of EC during MM progression excluding MM IFN signal.
- Supplemental Figure 8: Transcriptional remodeling of MSC during myeloma development in the MIcγ1 model.
- Supplemental Figure 9: Gene regulatory network of MSC during MM progression excluding MM IFN signal.
- Supplemental Figure 10: Cell-cell communication analysis between niche and PC.
- Supplemental Figure 11: Cell sorting strategy for isolation of human BM MSC.
- Supplemental Figure 12: Additional information on the transcriptional alterations of human MSC during myeloma progression.
- Supplemental Figure 13: Evaluation of MSC proportion in bulk RNA-seq human samples.

Supplemental Tables

- Supplemental Table 1: % infiltration of each mouse.
- Supplemental Table 2: DEGs between MGUS and control EC.
- Supplemental Table 3: DEGs between MM and MGUS EC.
- Supplemental Table 4: ORA between all stages MSC.
- Supplemental Table 5: DEGs between MGUS and control MSC.
- Supplemental Table 6: DEGs between MM and MGUS MSC.
- Supplemental Table 7: Full list of significant L-R pairs involved in EC and PC communication.
- Supplemental Table 8: Full list of significant L-R pairs involved in MSC and PC communication.
- Supplemental Table 9: Clinical characteristics of all individuals of bulk RNA-seq.
- Supplemental Table 10: Comparison between human MGUS-MSC and HD-MSC.
- Supplemental Table 11: Comparison between human MM-MSC and MGUS-MSC.
- Supplemental Table 12: Comparison between human MM -MSC and HD-MSC.